이학석사 학위논문

Synthesis and Optimization of CVD Graphene Films for Smart Applications

화학기상증착 그래핀의 스마트 필름 응용

2017년 8월

서울대학교 대학원

화학부 물리화학 전공

최 해 현

A Master Dissertation

Synthesis and Optimization of CVD Graphene Films for Smart Applications

화학기상증착 그래핀의 스마트 필름 응용

August 2017

Department of Chemistry
Graduate School of Seoul National University
Major: Physical Chemistry

Hae-Hyun Choi

Abstract

Synthesis and Optimization of CVD Graphene Films for Smart Applications

Hae-Hyun Choi
Physical Chemistry, Department of Chemistry
The Graduate School
Seoul National University

Many researchers have paid attention to various applications using graphene, a one-atom-thick planar sheet of sp^2-bonded carbon atoms, due to its exceptional mechanical, electronical and chemical properties. Here, we discuss interesting applications of graphene films grown by chemical vapor deposition (CVD) method from the point of physical and material chemistry. A brief overview of the chapters 1, 2 and 3 in this dissertation are shown below.

In chapter 1, we researched graphene barrier to prevent the decolorization of ink dye such as crystal violet (CV) under oxygen-rich condition. A quartz substrate coated with CV was placed under sunlight and the changes of absorbance in time-dependence were monitored for 7 days by Ultraviolet-visible spectroscopy, resulting from blue-violet to colorless. To analyze the effect of graphene films

under harsh condition, the absorbance changes of CV films covered with several stacking layer under UV/ozone were calculated. The absorbance ratio (A/A_0) of CV covered with 4-layer graphene is as low as 0.54 after 64 minutes under UV/O_3, which corresponds to 13 times compared to bare CV substrates. The graphene-passivated CV films exhibit attractive a prolong lifetime as well as environmental stability compared to the non-passivated the pigment film. We strongly confirm that graphene barriers not only prevent the oxidation of the dye but also decrease color change compared to no graphene on a pigment.

In chapter 2, we applied graphene heaters for real life through two heating mechanisms. First, to evaluate the powerful heating protocols and determine the more effective body region for heating, 4-layer graphene heaters were utilized in a cold environment, which conserved electrical power about 71% compared to continuous heating as well as achieved efficient the upper back heating. Secondly, the other heater was conducted in microwave condition because the electrons on graphene absorbed electromagnetic (EM) waves and released thermal energy. From this unique mechanism, graphene film was applied on a bottle glass using the smart defogging system through EM absorption.

In chapter 3, we controlled Fermi level of graphene by self-assembly monolayers with functional groups ($-NH_2$, $-CH_3$). We supposed that the electron donating property of amine group ($-NH_2$) promoted the reactivity than natural and p-doped graphene due to a mount of electrons on graphene. Interestingly, n-doped graphene enhanced the electrochemical reactivity of the surface functionalization and the synthesis of gold nanoparticles compared to other substrates. As the results, we expect to be able to use it for biosensors if we can functionalize and synthesize other attractive materials on graphene.

Keywords: Graphene application, Chemical vapor deposition, Self-assembled monolayer, Barrier, Heater. Reactivity

Student Number: 2015-20415

Table of Contents

List of Figures

Chapter 1.

Figure 1-7. (a, b) Optical image and Raman spectra of PET, CV/PET and CV/PET after oxidation respectively. (c, d) XPS spectra of integrated bonds before and after oxidation. (e, f) XPS spectra of 1C before and after oxidation.

Figure 1-8. (a) AFM image of graphene on CV/Si film. (b) Raman spectra of several types; PET, wet transferred graphene on PET, dry transferred graphene on PET and dry transferred graphene on CV film. Insert graph shows the magnification of 2D peaks. (c) Time-dependent relative absorbance ratio of CV/PET without graphene and with increasing graphene layers. Insert image shows color comparison of the initial color (left), no graphene and different graphene layers coated on CV/PET films after 64 minutes under UV/O_3 treatment. (d) Transmittance spectra of the change of CV film and 4-layer graphene/CV film after 64minutes under the harsh treatment.

Figure 1-9. Time dependent UV-Vis absorbance spectra about crystal violet degradation at different time durations using covered (a), no graphene (b), one layer (c), two layers (d), three layers and (e) four layers graphene.

Chapter 2.

Chpater 3.

Figure 3-1. (a) Controlling Fermi level of graphene by APTES and analysis via field effect transistor and Raman spectroscopy. (b) The comparing reactivity on functionalization of graphene surface due to the properties of underlying substrates.

Figure 3-2. (a) Molecular structures of amine-functionalized SAMs and methyl-functionalized SAMs on SiO_2/Si substrates and bare SiO_2/Si substrate. (b) Current-voltage characteristics of the graphene FETs on different SAMs-modified substrates. V_g: gate voltage; I_{sd}: source-drain current.

Figure 3-3. The illustration of calculated Fermi levels of each substrate by assuming -4.4 eV of standard graphene from the ref.20. Dashed lines indicate red: NH_2-SAM/SiO_2, black: CH_3-SAM/SiO_2, and blue: bare SiO_2.

Figure 3-4. Spatial Raman maps were collected for graphene on each substrate for the 28 μm × 28 μm regions in different substrates with 125 points in each map. (a) Representative Raman spectra of monolayer graphene on different substrates (b) D peak full-width at half-maximum (FWHM) versus D peak position. (c) I_{2D}/I_G intensity

ratio versus G peak position, with comparison data adapted from ref. 23 showing the doping trend. (d) 2D peak position versus G peak position distinguished literature[25]. Raman spectra were taken at 514 nm laser excitation wavelength.

Figure 3-5. (a) Representative Raman spectra of CVD-grown graphene deposited on different substrates before and after diazonium functionalization, normalized to the G peak height. (b) Raman map of I_D/I_G intensity ratio according to different substrates before and after diazonium functionalization, respectively.

Figure 3-6. (a) Optical image of alphabet G patterned substrate by e-beam lithography. (b) Optical image of graphene on APTES patterned on SiO_2/Si substrate. (c) Raman map of I_D/I_G intensity ratio before functionalization (or after APTES pattern) (d) Raman map of I_D/I_G intensity ratio after covalently functionalization.

Figure 3-7. (a-c) Bright field, dark field and SEM images of numerous gold nanoparticles placed on graphene/APTES, respectively. (d-f) Bright field, dark field and SEM images of a few gold nanoparticles placed on graphene, respectively. (g-i) Bright field, dark field and SEM images of plenty of gold nanoparticles placed on graphene, respectively. Scale bars at the bottom right of

each image.

Figure 3-S1. 2D peak FWHM versus 2D peak position, showing different clusters depending on substrates.

Figure 3-S2. The illustration of patterning process for alphabet G pattern using e-beam lithography. After patterned PMMA/SiO_2 immerged in APTES solution to block deposition of SAMs on the substrate, PMMA was removed in acetone. Then graphene was transferred onto SAMs-patterned substrate.

List of Tables

Chapter 1.

Chapter 3.

Chapter 1. Preventing Decolorization of Inkjet Printed Photographs by Graphene Barrier Films

1.1. Abstract

Graphene have afforded to prohibit the penetration of gases and liquids due to ordered packing structure as a barrier film. Here we transferred graphene layers synthesized by chemical vapor deposition (CVD) onto an ink pigment such as crystal violet (CV) through dry transfer method because it can be applied to inkjet printed photographs. To analyze an effect of graphene barrier, the absorbance at 600 nm of CV films covered with several stacking layer was measured under sunlight and UV/ozone by the Ultraviolet-visible spectroscopy. Furthermore, stability test under harsh oxygen-rich conditions was conducted by applying UV/ozone treatment (λ = 254 nm) to the ink films. The absorbance ratio (A/A_0) of CV covered with 4-layer graphene was calculated to be as low as 0.54 after 64 minutes under UV/O_3, which corresponded to 13 times compared to bare CV substrates. The graphene-passivated CV films exhibit a prolong lifetime as well as distinguished environmental stability compared to the nonpassivated the pigment film. We expect graphene films to protect photodegradation of inks on paper and pictures in the future.

1.2. Introduction

Graphene, as an allotrope of carbon in a two-dimension with hexagonal lattice, has received much attention and motivated researchers to develop new innovative technologies in recent years due to its excellent chemical, electrical and mechanical properties[1-5]. In addition, it remarkably possesses unique barrier properties with high optical transmittance in the visible range up to 97.7%[6]. Therefore, it has been regarded as a flexible and protective coating material to prevent the penetration of gases and liquids due to its ordered packing structure[7-11]. Generally, inorganic materials such as aluminum oxides (Al_2O_3) and silicone oxides (SiOx) have been mostly employed as the barrier films, but the poor mechanical flexibility of these materials has hindered the flexible applications[12-14]. In this regard, graphene films, reduced graphene oxide (RGO) and graphene hased heterostructures with excellent water impermeability, flexiblity, and transmittance are expected to be useful for more reliable and durable barrier of an organic device shown in Figure 3-1.

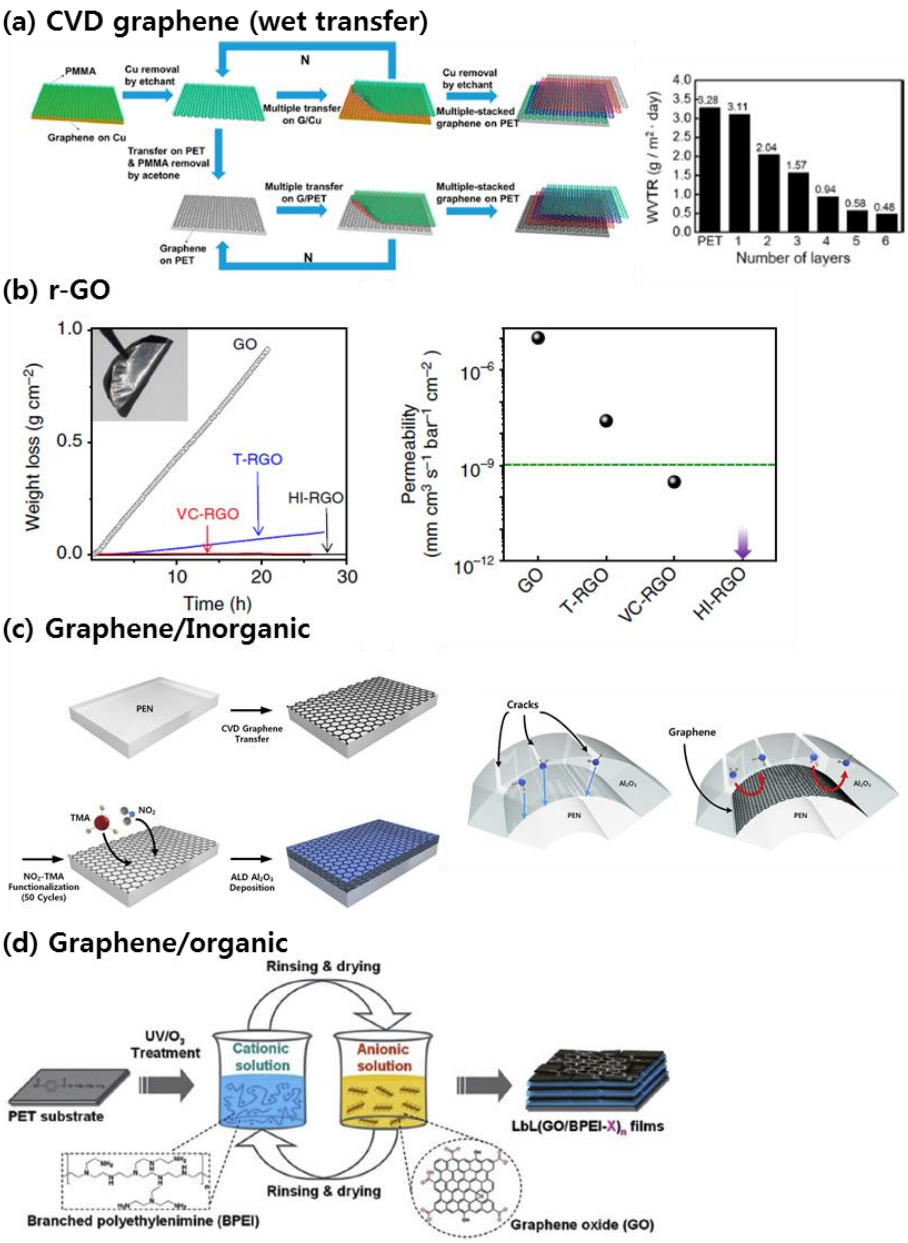

Figure 1-1. Various types of grphene barriers. (a) CVD graphene barrier stacked by wet transfer[15]. (b) Reduced graphene oxide[16]. (c) Graphene/Al_2O_3 films[17]. (d) BPEI/graphene oxide films[18].

Recently, Choi *et al.* have successfully demonstrated that the large-size graphene films stacked by wet transfer could cover an organic field-effect transistor (OFET) and were measured by the water vapor transmission rate (WVTR)[15]. However, the wet transfer is impossible to transfer water-soluble materials such as inks on a substrate as well as highly causes mechanical damages via the microscopic tears[19]. Therefore, using thermal release tape (TRT) can be replaced with wet transfer, which is able to transfer on organic films without water[20].

Here, we transfered several graphene films on CV solution in air-dried by TRT method using lamination (see Methods for details). To investigate graphene barrier property, we had monitored the degradation of CV pigment, which is easily degradble under sunlight and widely used as ink materials. CV films were under ambient and UV/Ozone condition and measured by UV-vis spectroscopy to obatin absorbance (a.u.) and transmittance (%). To comapre initial state with oxidized dye, we calculated absorbacne ratio (A/A_0) of 4-layer graphene on PET/CV film and bare PET/CV, which are 0.54 and 0.04 respectively. We also analyzed XPS spectrum before and after oxidation, resulting in broaden peaks at 1S carbon.

1.3. Experimental Section

Chemicals. Crystal Violet (CV, $C_{25}H_{30}ClN_3$, 90%) from Alfa-Aesar; Poly(methyl methacrylate) (PMMA, $(C_5O_2H_8)_n$), ammonium persulfate ($(NH_4)_2S_2O_8$) from Sigma-Aldrich; ethanol, acetone, IPA from Samchun Pure Chemicals; and Thermal release tape (TRT) films and Polyethylene-terephthalate (PET) from Jinsung Ins.; Deionized water from Purescience Ins. was used throughout the experiments.

Synthesis of CVD Graphene. A large size of graphene was grown on Cu foil using vertical CVD method which use hydrogen (4 sccm) and methane (40 sccm) gases in a qurtz tube. The Cu foil was inserted into the vertical CVD and heated to 1000 °C under H_2 flow. Then, CH_4 was injected into the tube to grow a monolayer graphene for 30 min. Finally, The tube was cooled down to room temperature under H_2. The one side of graphene on Cu foil was removed by reactive ion etching (RIE) and thermal release tape (TRT) was placed on the other side graphene film by lamination. The Cu foil was eliminated by Cu etchant (0.08 M ammonium persulfate). This method was modified from ref. 20.

Crystal violet films. PET films were immersed in 500 μM and 5 mM of Crystal violet and ethanol solution for 1 hour. Then, the PET films

coated with CV were dried. While one side of PET/CV was removed with ethanol, the other side was covered with several graphene layers by the lamination.

Preparation of XPS and AMF samples. 5 mM of Crystal violet solution dropped onto ultraclean Si/SiO2 substrates and dried. To investigate the UV/Ozone effect, dried CV on the substrates were irradiated UV in the presence of oxygen species.

Characterization. Atomic force microscopy (AFM) images were collected in the noncontact mode using Park system XE-100. X-ray photoelectron spectroscopy (XPS) spectra, ^{1}H-NMR was measured by Bruker Avance III 300MHz with $CDCl_3$ as solvent. Raman spectroscopy was performed using a Renishaw 2000 (excitation at 514.5 nm)

1.4. Results and Discussion

We dried crystal violet solution, which is soluble and photodegradable organic pigment [21], on several substrates to examine the barrier property of graphene. Grown-graphene using a typical CVD method with flowing 40 sccm methane and 4 sccm hydrogen gases at 1000 °C was transferred on TRT by soft rollers, followed by etching with APS solution. TRT/Graphene films applied on crystal violet in air-dried on substrates and released under 110 °C (Figure 1-2).

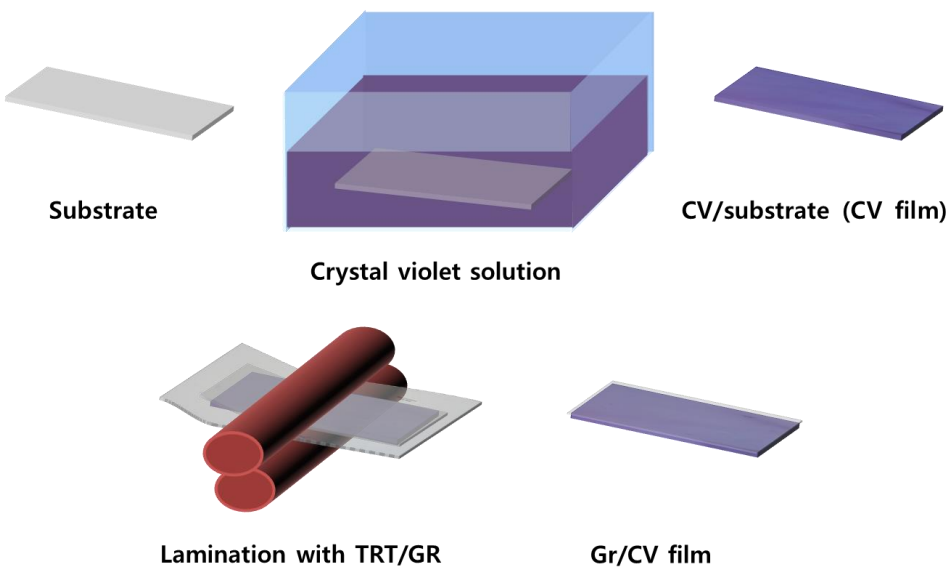

Figure 1-2. Schematic illustration of crystal violet onto a target

substrate and the transfer process.

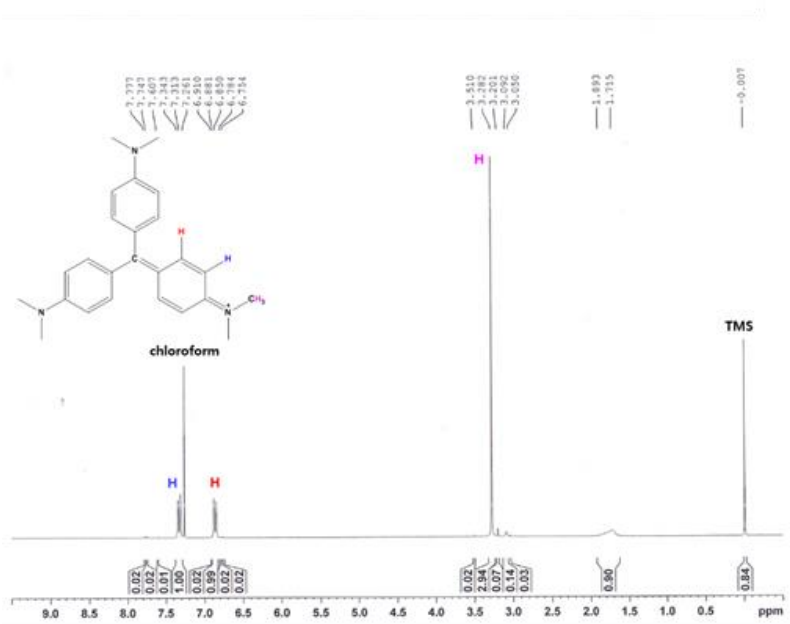

Figure 1-3. ^{1}H-NMR spectra of crystal violet molecules.

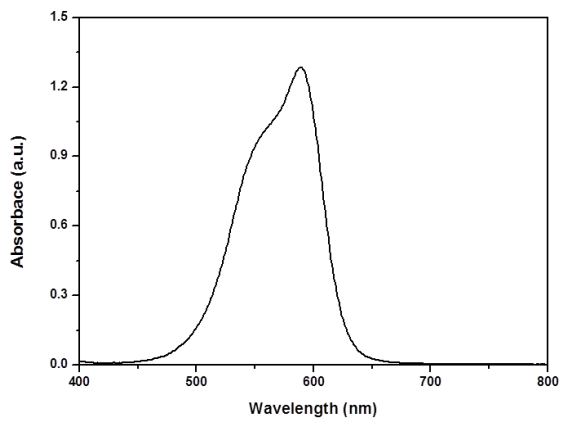

Figure 1-4. Absorbance spectra of crystal violet in ethanol.

CV was used in this work to examine the barrier property of graphene. To analyze CV molecules, its structure and optical property were measured by ^{1}H-NMR (Figure 1-3) and UV-Vis spectroscopy (Figure 1-4), respectively. As the results, it exactly coincides with the structure and absorbance of crystal violet.

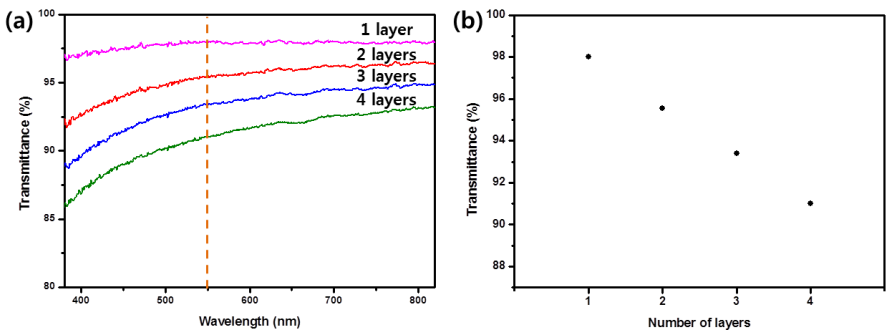

Figure 1-5. (a) UV-Vis spectra of different graphene layers in visible region. (b) Transmittance(%) at 550 nm of graphene films on PET with increasing number of graphene layers. 1st: 98.0%; 2nd: 95.5%; 3rd: 93.4% 4th: 91.0%.

To investigate the multi-stacked graphene layers, it should be noted that the graphene layers performance a superb optical transmittance in visible region (Figure 1-5a, b), which is the most important for the barrier of various optoelectronic applications. To

examine the morphology of CV/Si film, 1mM of Crystal violet in ethanol solution dried onto Si substrate under air and was analyzed by SEM and AFM shown in Figure 1-6a, b. Consequentially, CV exits on the target substrate with roughness by drop-casting. Furthermore, the absorbance change of CV on quartz had monitored for 7 days under sunlight by UV-Vis spectroscopy (Figure 1-6c). As the result, the organic pigment was damaged in ambient air and light (Figure 1-6d). However, when compared to its absorbance in solution, absorption spectra of CV in film is broadly displayed and slightly difference at the absorption maxima due to the changes of the spectra induced by the crystal structure and the coupling of the molecules[22]. Therefore, the wavelength at maximum absorbance is changed to red shift by effects of reducing the intermolecular interaction which lead to poorer π-stacking during the dry process.

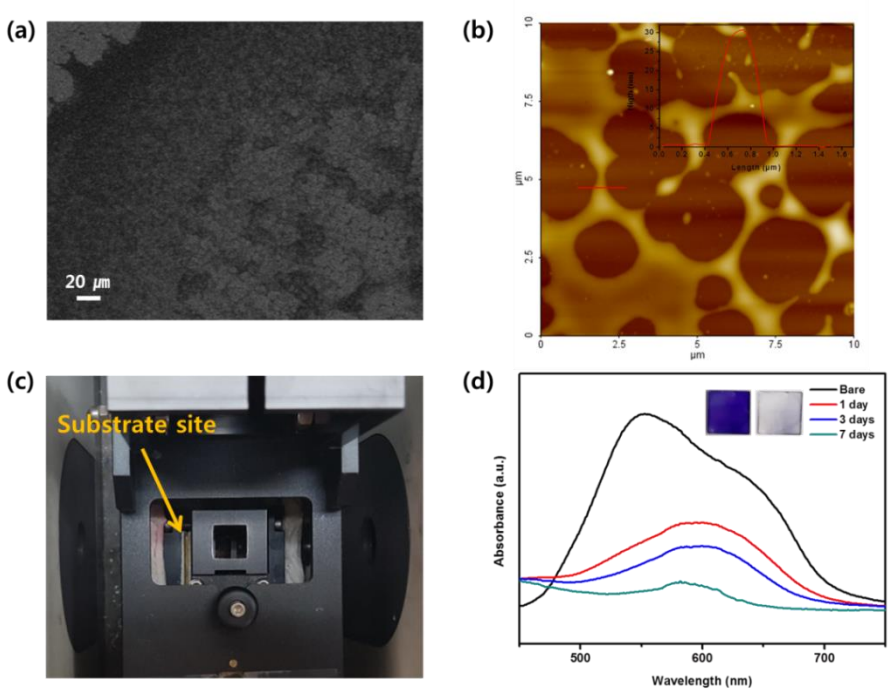

Figure 1-6. (a,b) SEM and AFM images of CV on Si substrate. insert graph; the CV height. (c) Optical image of UV-Vis spectroscopy (d) Absorption spectra of CV on quartz for 7 days in the ambient condition. Insert lines shows initial, 1, 3 and 7 days after, respectively.

Instead of sunlight experiment, stability tests under harsh oxygen-rich conditions were conducted by applying UV/Ozone treatment (λ = 254 nm) called ozonolysis, which is an organic reaction where the unsaturated bonds are cleaved with ozone and oxidized [21]. This is

the formula of ozonlysis for crystal violet molecules in below. The crystal violet molecule absorbs ultraviolet radiation, and, as it does, becomes excited and it raised to a higher energy state than normal. In addition, oxygen species easily attacks bonds and then CV is broken, resulting in gases.

$$
\begin{aligned}
&CV + h\nu \rightarrow CV^* \\
&O_2 + h\nu \rightarrow 2O^* \\
&O^* + O_2 \rightarrow O_3 \\
&O_3 + h\nu \rightarrow O^* + O_2 \\
&CV^* + (O^*, O_3) \rightarrow CO_2 + H_2O + N_2
\end{aligned}
\qquad \text{Formula-(1)}
$$

PET films, which are the most popular substrate with flexibility and transparency, were dip-coated on CV solution and dried up. Figure 1-7a, b show the optical images and Raman spectra of the CV change under harsh condition for 30 minutes, resulting in considerable decreasing in characteristic peaks of the dye molecules. These oxidation and degradation behaviors depended on the exposure time and were further examined by X-ray photoemission spectroscopy (XPS) shown in Figure 1-7 c-f. The XPS spectra of CV indicates carbon peaks related to non-oxidation before the treatment, whereas those of oxidized CV are shown in the broad peaks corresponding to oxide (C 1s N-C=O, 288.09 eV) as reported by the ref. 24. In addition, Table 1-1 is consistent with the oxidation of CV due to the change of atom percentage (%).

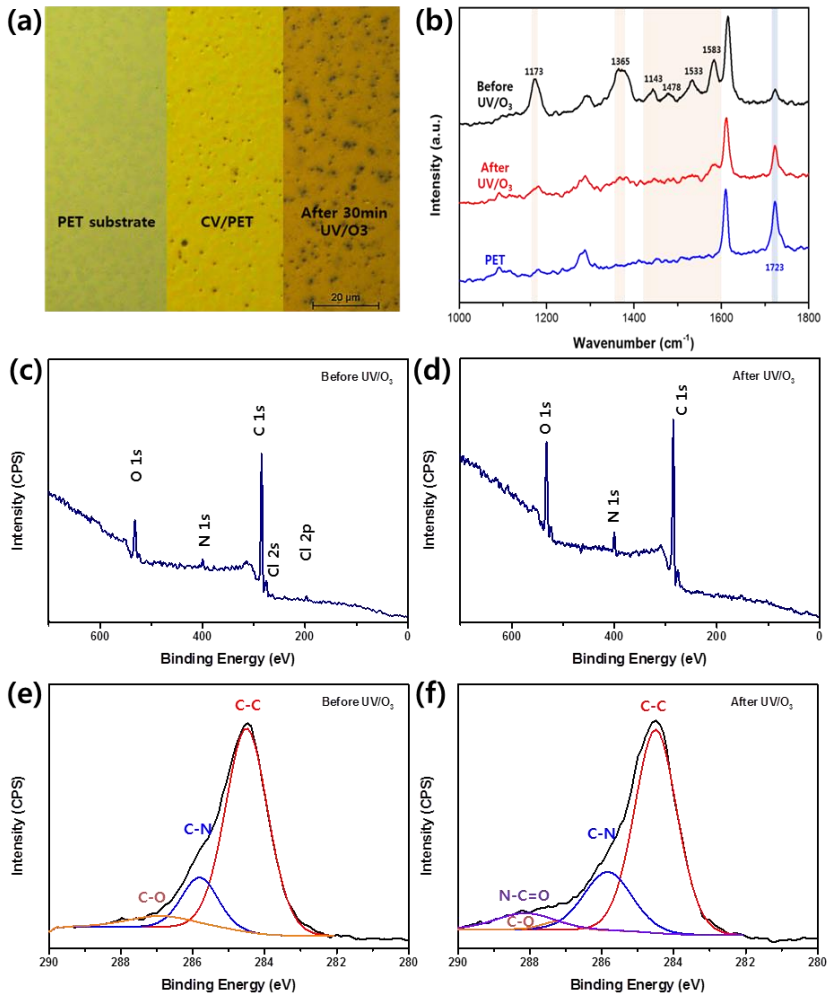

Figure 1-7. (a, b) Optical image and Raman spectra of PET, CV/PET and CV/PET after oxidation respectively. (c, d) XPS spectra of integrated bonds before and after oxidation. (e, f) XPS spectra of 1C before and after oxidation.

Sample	C 1s	N 1s	O 1s
Before UV/O_3	284.48	399.58	531.78
	(85.52%)	(4.82%)	(12.37%)
After UV/O_3	284.8	399.8	532.5
	(75.51%)	(6.28%)	(18.21%)

Table 1-1. Binding energies in eV and atom concentration percent (%) from XPS spectra of CV before and after oxidation.

To confirm the existence of graphene sheet on CV, we used silicon substrate with flatness more than PET. Graphene was transferred on it and investigated by atomic force microscopy (AFM) shown in Figure 1-8a. Undoubtedly, CV is covered with graphene film, recognizing the height of graphene layer and dried dye on Si substrate. In addition, Figure 1-8b shows the Raman spectra of the PET and others. Compared with graphene transferred by wet method, graphene transferred via the TRT method is well performed. Moreover, comparing the inserted 2D peak around 2680 cm^{-1} reveals that graphene is on CV/PET. From this data, both wet transfer and dry transfer are well conducted. Figure 1-9a-f indicate the degradation of crystal violet on flexible PET films under the harsh condition as time-dependence. As said upper, the stacking molecules

during the air-dry were red shifted, showing the maxima absorbance from 590 nm to 600 nm. The absorbance ratio (A/A_0) of bare film was calculated to be as low as 0.04 after 64 minutes under UV/O_3, while 4-layers graphene barrier corresponded to 0.54 at 600 nm (Figure 1-8c). Also, we obtained change of transmittance (%) by UV-Vis spectrometer in Figure 1-8d. As the result, the graphene-coated CV films exhibit excellent environmental stability as well as a prolong lifetime compared to the non-coated the pigment film. We further infer that graphene can act as an anti-oxidation layer due to its densely packed structure that does not permit the transmission of gases or liquids.

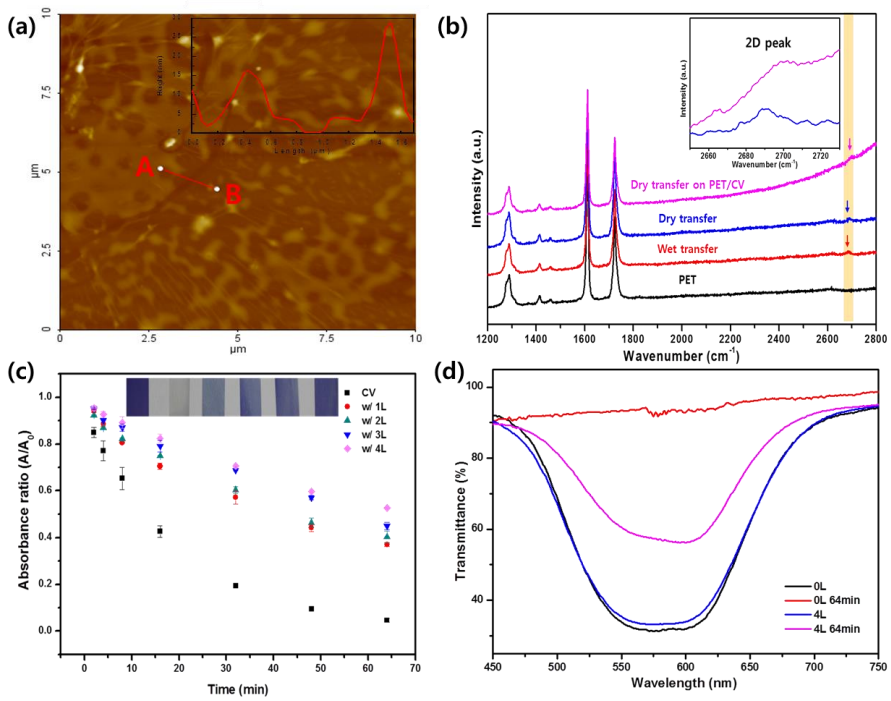

Figure 1-8. (a) AFM image of graphene on CV/Si film. (b) Raman spectra of several types; PET, wet transferred graphene on PET, dry transferred graphene on PET and dry transferred graphene on CV film. Insert graph shows the magnification of 2D peaks. (c) Time-dependent relative absorbance ratio of CV/PET without graphene and with increasing graphene layers. Insert image shows color comparison of the initial color (left), no graphene and different graphene layers coated on CV/PET films after 64 minutes under UV/O_3 treatment. (d) Transmittance spectra of the change of CV film and 4-layer graphene/CV film after 64minutes under the harsh treatment.

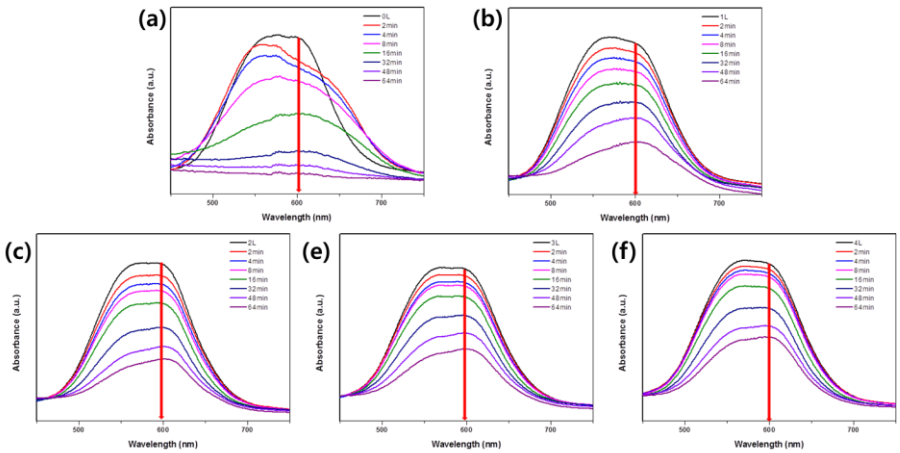

Figure 1-9. Time dependent UV-Vis absorbance spectra about crystal violet degradation at different time durations using covered (a), no graphene (b), one layer (c), two layers (d), three layers and (e) four layers graphene.

When graphene film was applied to a photograph in order to confirm that it could prevent the degradation of the inks under sunlight, the coated-photo show less color change than the uncoated-photo (Figure 1-10 a-c). Compared to the picture with graphene, pupil and hair colors on uncoated picture were dramatically changed by sunlight and indicated by different red-green-blue (RGB) values shown in Figure 1-10 (d,e).

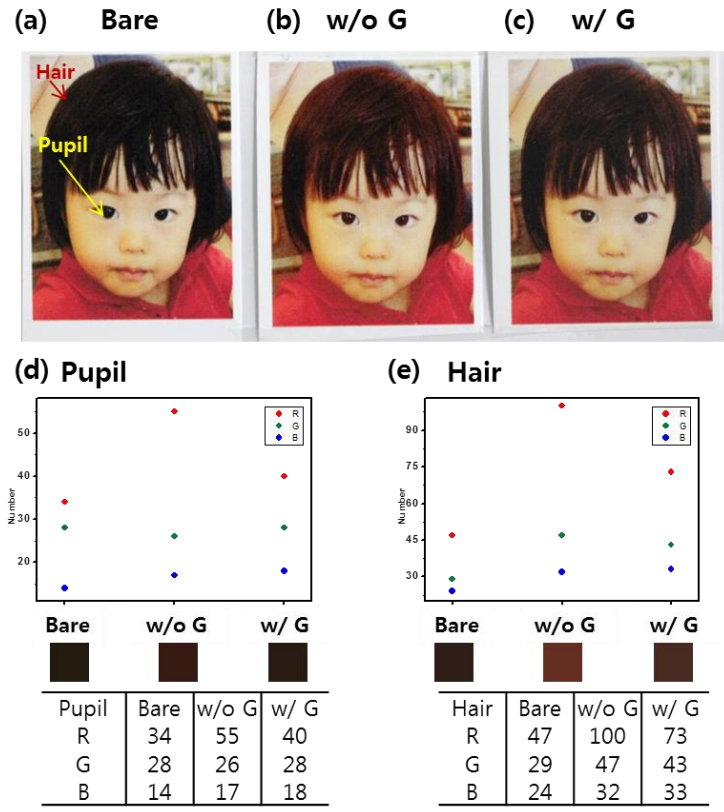

Pupil	Bare	w/o G	w/ G
R	34	55	40
G	28	26	28
B	14	17	18

Hair	Bare	w/o G	w/ G
R	47	100	73
G	29	47	43
B	24	32	33

Figure 1-10. The photograph without graphene (a) and exposed photos under sunlight for one day (b: uncoated picture, c: coated picture).

1.5. Conclusions

In summary, we have successfully conducted the barrier effect of four layers graphene on dried organic film under UV/Ozone condition, resulting in a 13-fold improvement compared to the CV/PET film. The XPS and Raman spectra revealed that the graphene films are well transferred on PET by dry transfer and efficiently protect the discoloration of organic molecules from oxygen species. We believe that our results provide an important barrier on paintings and pictures which contain organic inks. Finally, further work is required to eliminate the residue on graphene surface and develop the most proper methods for dry transfer without thermal energy during the fabrication process.

1.6. Acknowledgments

This work was financially supported by a research grant from LG Display.

1.7. References

[1] Geim, A. K.; Novoselov, K. S. *Nat. Mater.* 2007, **6**, 183-191.

[2] Lee, C.; Wei, X.; Kysar, J. W.; Hone, J. *Science* 2008, **321**, 385-388.

[3] Koenig, S. P.; Boddeti, N. G.; Dunn, M. L.; Bunch, J. S. *Nat. Nanotechnol.* 2011, **6**, 543-546.

[4] McAllister, M. J.; Li, J.-L.; Adamson, D. H.; Schniepp, H. C.; Abdala, A. A.; Liu, J.; Herrera-Alonso, M.; Milius, D. L.; Car, R.; Prud'homme, R. K. *Chem. Mater.* 2007, **19**, 4396-4404

[5] Wang, X.; Li, X.; Zhang, L.; Yoon, Y.; Weber, P. K.; Wang, H.; Guo, J.;Dai,H. *Science* 2009, **324**, 768-771.

[6] Z. Liu, J. Li, Z. Sun, G. Tai, S. Lau and F. Yan *ACS Nano*, 2012, **6**, 810-818

[7] Bunch, J. S.; Verbridge, S. S.; Alden, J. S.; van der Zande, A. M.; Parpia, J. M.; Craighead, H. G.; McEuen, P. L. *Nano Lett.* 2008, **8**, 2458-2462.

[8] Nair, R. R.; Wu, H. A.; Jayaram, P. N.; Grigorieva, I. V.; Geim, A. K. *Science* 2012, **335**, 442-444

[9] Liu, Z.; Li, J.; Yan, F. *Adv. Mater.* 2013, **25**, 4296-4301.

[10] Su, Y.; Kravets, V. G.; Wong, S. L.; Waters, J.; Geim, A. K.; Nair, R. R. *Nat. Commun.* 2014, **5**, 4843.

[11] Celebi, K.; Buchheim, J.; Wyss, R. M.; Droudian, A.; Gasser, P.; Shorubalko, I.; Kye, J.-I.; Lee, C.; Park, H. G. *Science* 2014, **344**, 289-292

[12] Li, D.; Borkent, E.-J.; Nortrup, R.; Moon, H.; Katz, H.; Bao, Z. *Appl. Phys. Lett.* 2005, **86**, 042105

[13] Jeon, H.; Shin, K.; Yang, C.; Park, C. E.; Park, S.-H. K. *Appl. Phys. Lett.* 2008, **93**, 163304.

[14] Meyer, J.; Görrn, P.; Bertram, F.; Hamwi, S.; Winkler, T.; Johannes, H.-H.; Weimann, T.; Hinze, P.; Riedl, T.; Kowalsky, W. *Adv. Mater.* 2009, **21,** 1845-1849

[15] Choi K.; Nam S.; Lee Y.; Lee M.; Jang J.; Kim S. J.; Jeong Y. J.; Kim H.; Bae S.; Yoo J. B. ; Cho S. M; Choi J.B.; Chung H.K.; Ahn J.H.; Park C.E.; Hong B.H. *ACS Nano*, 2015, **9**, pp 5818-5824

[16] Y. Su; V.G. Kravets; S.L. Wong; J. Waters; A.K. Geim and R.R. Nair, *Nature Com.*, 2014, **5**, 4843

[17] T. Nam; Y. J. Park; H. Lee, I. K. Oh; J. H. Ahn; S. M. Cho; H. K. and H.B.R. Lee *Carbon*, 2017, **116**, 553-561

[18] J.T. Chen, Y.J. Fu, Q.F. An, S.C. Lo, S.H. Huang, W.S. Hung, C.C. Hu, K.R. Lee, J.Y. Lai, *Nanoscale,* **5 (19)**, 2013, 9081-9088.

[19] Kim S.J.; Choi T.; Lee B.; Lee S.; Choi K; Park J.B.; Yoo J.M.; Choi Y.S.; Ryu J.; Kim P.; Hone J.; Hong B.H. *Nano Lett.,* 2015, **15** , pp 3236-3240

[20] Bae, S.; Kim, H.; Lee, Y.; Xu, X.; Park, J.-S.; Zheng, Y.; Balakrishnan, J.; Lei, T.; Ri Kim, H.; Song, Y. I. *Nanotechnol.* 2010, **5**, 574-578.

[21] AK Gupta; A Pal; C Sahoo *Dyes and Pigments*, 2006, 69(3), 224-232

[22] Alexander H.; Ute H,; Alexander G.; Stefan K.; Robert M. J.; Youichi S.; Toshyuasu S.; Frank S.; *J. Chem. Phys.*, 2007, **127**, 194705

[23] Rudolf Criegee, *Angew. Chem. Internat.*, 1975, **14(11)**, 745-752

[24] Ptasińska S.; Stypczyńska A.; Nixon T.; Mason N.J.; Klyachko; Sanche L. *J. Chem. Phys.* 2008, **129**, 065102

Chapter 2. CVD Graphene Films for Smart Heating Applications

2.1. Introduction

Graphene has been well known due to its excellent physical[1,2] and chemical[3] properties. In addition, optical and thermal researches have shown that monolayer graphene film transmits light in the visible range and easily spreads heat energy to surrounding. Graphene exhibits further advantageous characteristics such as remarkably high elasticity and chemical stability, whereas transparent indium thin oxide does not[4-6]. These particular properties faciliate graphene films to be transparent heater[7,8] with flexibility on curved surface such as glasses and elastomeric substrates, where metal oxides cannot be applicable because of their brittleness shown in Figure 2-1.

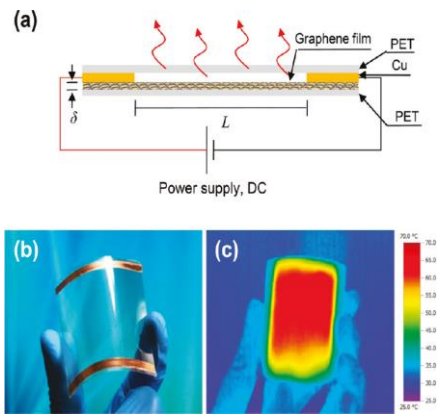

Figure 2-1. (a) An illustration of a light and flexible graphene heater with PET substrate and Cu electrodes. (b) A photograph of graphene-based heater. (c) An infrared picture of graphene heater

while applying an input voltage from reference[7].

To use graphene films in various applications, it is crucial to develop high technology to produce large-size graphene and continuous films with a controlled number of layers. In 2004, High-quality graphene monolayers were successfully obtained by mechanical exfoliation[1]. However, this method can only provide micro-sized graphene flakes without controllability and scalability[9]. Meanwhile chemical vapor deposition (CVD) graphene on metal[4] has introduced monolayer graphene films to be used for diverse applications because of large-size graphene with lightness, flexibility and transparency. Furthermore, the transfer methods are critical to promote the research in real world[10]. Among transfer methods, dry transfer has been developed using thermal release tapes (TRTs) and pressure sensitive adhesive films (PSAFs)[11].

Herein, we synthesized large-area graphene using vertical CVD and then graphene films were used as heaters by high-current Joule heating and absorption electromagnetic waves to use applications from laboratory to life. First, we applied graphene heater to cold protective clothing for evaluation of heating protocols. This was a study that has been applied to eight people unlike other research. Secondly, we suggested a new concept of graphene heater

mechanism interpreted with the absorption of electromagnetic (EM) waves, inducing the movement of electrons on graphene. For this phenomenon, fast heating of graphene films by EM waves can be used to remove the fog or moisture from a window called defogging [12].

2.2. Graphene heater for cold protective clothing by Joule heating

Body cooling mechanism effects on physical and mental performance in various ways[13]. Physiological response to body temperature included in falling and shivering, etc. The prolonged cold could cause a range of cold injury and illness such as cracked skinand frostbite[14,15]. This study was the purpose of evaluation for the effects of intermittent and continuous heating protocols using graphene heaters. Furthermore, we identified the more useful body region for heating in cold surroundings. We fabricated high-performance and flexible graphene heaters through multiple transfers and chemical doping process[7]. These graphene heaters were conducted by Joule heating which is the process by the movement of current through a conductor releases heat due to tis resistance[12].

Large-size graphene was synthesized utilizing vertical CVD process described in the chapter 1. The graphene film grown on the copper foil was covered by thermal release tape (TRT) and floated in the Cu etchant (0.08 M ammonium persulfate). Graphene/TRT was transferred on a clean Polyethylene-terephthalate (PET) substrate by a lamination. Finally, the TRT could be easily released after rolling process at 110 ℃[7]. The graphene on PET carried out the

multiple stacking processes by the soft rollers. After attaching Cu tapes as an electrode on two edges of the 4-layer graphene film, we finally fabricated graphene heater with coating cover (Figure 2-2a). The weight and size was 5.8 ± 0.4 g and (5.7 ± 0.4 cm) × (10.5 ± 0.5 cm), respectively (Figure 2-3b top). Graphene heaters were inserted between underwear and skin with temperature measurement (Figure 2-2b).

To analyzed surface of graphene, we obtained SEM image, which are shown in Figure 2-3a. Furthermore, the surface of temperature distribution was characterized by an infrared thermography camera (Figure 2-3b bottom).

To sum up the experiment, we followed various conditions and circumstances to maintain psychological comfort using the thinnest and flexible graphene heaters in the cold environment. We have achieved two results: (1) the upper back heating was more effective than the chest heating. (2) the intermittent heating protocol conserved electrical power as much as 71% compared to continuous heating. This experiment was carried out with the department of textiles.

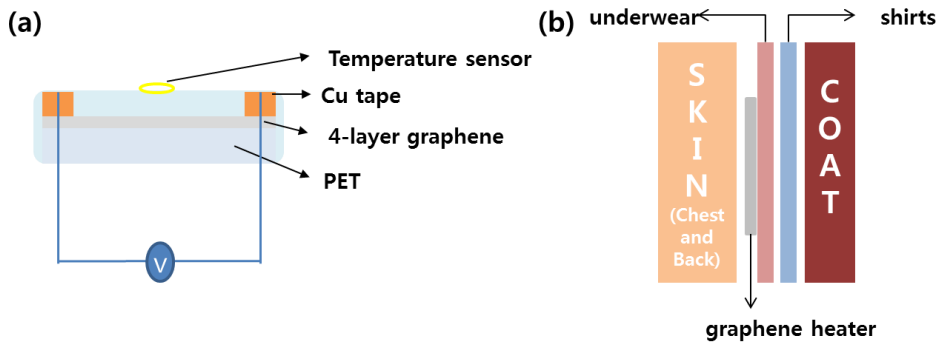

Figure 2-2. (a) A Scheme for the graphene heater and (b) the position of graphene heater.

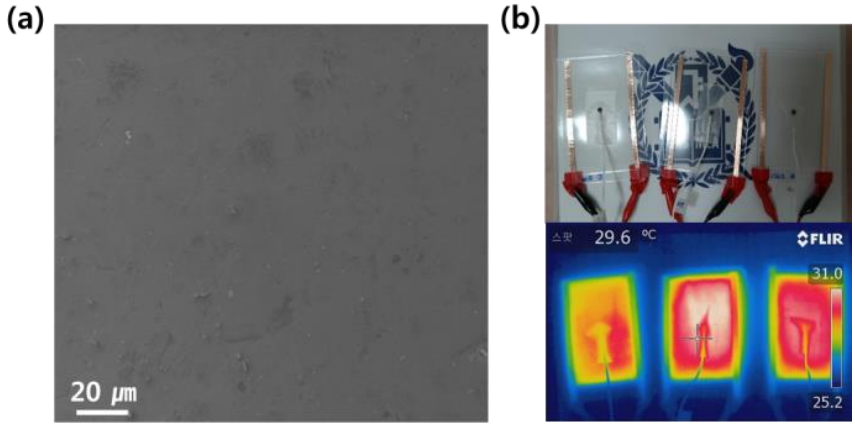

Figure 2-3. SEM image of the surface on 4-layer graphene (a) and the optical and thermographic image of graphene heaters (b).

2.3. Graphene heater for defogging by absorption of electromagnetic wave

Graphene has super thermal conductivity which leads to many applications followed in Joule heating mechanism[7,8]. However, we here suggested that graphene sheet was heated by absorption property for electromagnetic (EM) waves such as microwave. We performed multi-stacked graphene via single PMMA coating/removal step[16] and applied to several substrates.

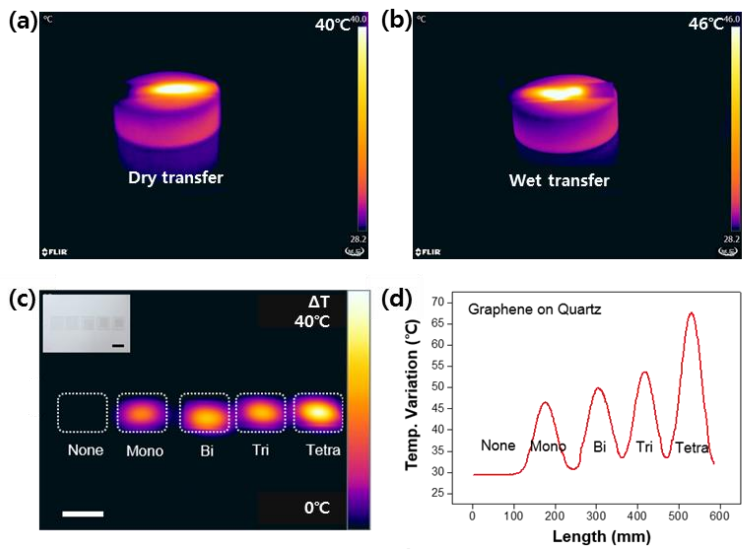

Figure 2-4. (a, b) Infrared photographs showing the difference between dry and wet transfer when heated by microwave, respectively. (c) The temperature change depending on the number of layers on quartz substrates. (d) The change of temperature depending on graphene layers.

First of all, to verify the thermal effect of water trapped between graphene and different substrates[17], we tested dry and wet transferred graphene films in a microwave oven (Figure 2-4a, b). This result indicates that the effect of water via wet transfer is negligible compared to dry transfer. Especially, graphene sheets on quartz substrates were easily heated with the proportion to layers, resulting in the change of temperature was depending on the number of graphene layers (Figure 2-4c, d). As the result, the EM waves can induce the electron movement in graphene, resulting in thermal energy on the graphene surface by oscillating moment.

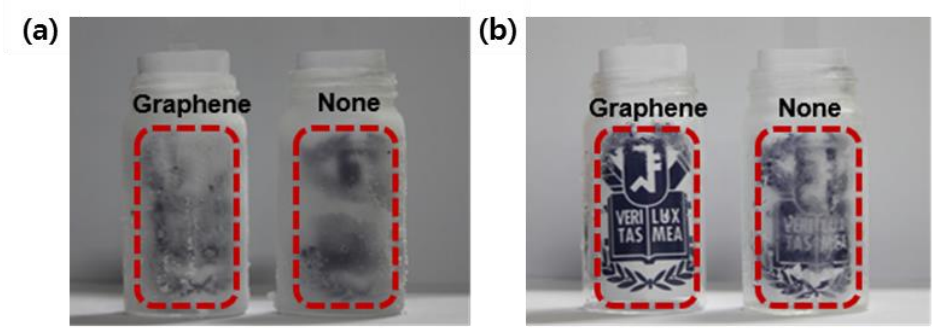

Figure 2-5. The photograph showing defrosting test results of graphene coated (left) and uncoated (right) vials. (a) Frost formation and (b) after microwave irradiation during 5 seconds. [12]

We expected that graphene could be used in smart defogging application because quartz is one of the glasses. After non-coated vial and the graphene-coated vial were prepared, these were in the freezer to have frost on the surfaces. Irradiated by microwave for 5 seconds, the graphene-passivated bottle was completely clear compared to the non-passivated bottle (Figures 2-5a, b)[12]. This result shows that graphene is easily heated by EM and transferred on curved surface. This suggests that the graphene heater by EM waves is applicable to smart windows and EM wave detectors[12].

2.4. References

[1] Geim, A. K.; Novoselov, K. S. *Nat. Mater.* 2007, **6**, 183-191.

[2] Novoselov, K. S.; Geim, A. K.; Morozov, S. V.; Jiang, D.; Zhang, Y.; Dubonos, S. V.; Grigorieva, I. V.; Firsov, A. A *Science*, 2004, **306**, 666-669

[3] Wang, X.; Li, X.; Zhang, L.; Yoon, Y.; Weber, P. K.; Wang, H.; Guo, J.; Dai, H. *Science*, 2009, **324**, 768-771.

[4] Kim, K. S.; Zhao, Y.; Jang, H.; Lee, S. Y.; Kim, J. M.; Kim, K. S.; Ahn, J. H.; Kim, P.; Choi, J. Y.; Hong, B. H. *Nature,* 2009, **457**, 706-710

[5] Li, X. S.; Cai, W. W.; An, J. H.; Kim, S.; Nah, J.; Yang, D. X.; Piner, R. D.; Velamakanni, A.; Jung, I.; Tutuc, E.; Banerjee, S. K.; Colombo, L.; Ruoff, R. S. *Science*, 2009, **324**, 1312-1314.

[6] Reina, A.; Jia, X.; Ho, J.; Nezich, D.; Son, H.; Bulovic, V.; Dresselhaus, M. S.; Kong, *J. Nano Lett.*, 2009, **9**, 30-35.

[7] J. Kang, H. Kim, K. S. Kim, S. Lee, S. Bae, J. H. Ahn, Y. J. Kim, J. B. Choi, and B. H. Hong, *Nano Lett.,* 2011, **11**, 5154-5158

[8] J. Kang, Y. Jang, Y. Kim, S. H. Cho, J. Suhr, B. H. Hong, J. B. Choi and D. Byun, *Nanoscale*, 2015, **7**, 6567-6573

[9] J. M. Lee; H. Y. Jeong; W. I. Park, *J. Electronic Materials*, 2010, **39 (10)**, 2190-2195

[10] S. Bae, H. Kim, Y. Lee, X. Xu, J. S. Park, Y. Zheng, J. Balakrishnan, T. Lei, H. R. Kim, Y. I. Song, Y. J. Kim, K. S. Kim,

B. Özyilmaz, J. H. Ahn, B. H.Hong, S. Iijima, *Nature Nanotech.* 2010, **5,** 574

[11] S. J. Kim, T. Choi, B. Lee, S. Lee, K. Choi, J. B. Park, J. M. Yoo, Y. S. Choi, J. Ryu, P. Kim, J. Hone, and B. H. Hong, *Nano Letters,* 2015, **15,** 3236–3240.

[12] S. Kang, H. Choi, S. B. Lee, S. C. Park, J. B. Park, S. Lee, Y. Kim and B. H. Hong " *2D Mater.,* 2017, **4**, 025037

[13] V. P. Raatikka, M. Rytkönen, S. Näyhä, J. Hassi, Int. *J. Bioneteirol*. 2007, **51,** 441

[14] D. W. DeGroot, J. W. Castellani, J. O. Williams, P. J. Amoroso, Aviat. *Space. Environ. Med.,* 2003, **74,** 564.

[15] T. M. Mäkinen, J. Jokelainen, S. Näyhä, T. Laatikainen, P. Jousilahti, J. Hassi, Scand. J. Work, *Environ. Health.*, 2009, **35**, 384

[16] Choi K.; Nam S.; Lee Y.; Lee M.; Jang J.; Kim S. J.; Jeong Y. J.; Kim H.; Bae S.; Yoo J. B. ; Cho S. M; Choi J.B.; Chung H.K.; Ahn J.H.; Park C.E.; Hong B.H. *ACS Nano*, 2015, **9**, pp 5818–5824

[17] Y. Kim; D. H. Cho; S. Ryu; C. Lee, *Carbon*, 2014, **67,** 673–679,

Chapter 3. Tuning the Electrochemical Reactivity of Graphene by Self-Assembled Monolayers for Enhancing Reactivity

3.1. Abstract

The chemical doping of graphene has been much investigated due to the control of electronic and chemical properties, which provides an effect on the surface modification of graphene. Herein, we performed that the properties of doped graphene by self-assembly monolayers (SAMs) were measured via field effect transistors (FETs) and Raman spectroscopy. Dirac point of n-type graphene was – 160 V corresponding to 0.43 eV of Fermi level due to the electron-donating NH_2-terminated SAMs inducing strong n-doping in graphene. Also, the change of peaks depending on surface properties was monitored via Raman map. As anticipated, the electron density of graphene plays a key role in electrochemical reactivity by electron-transfer. For example, n-doped graphene can be easily functionalized by diazonium salts due to abundant electrons on n-type graphene. Furthermore, we synthesized gold nanoparticles on different graphene films. As the result, we found that amount of electrons of graphene has an effect on reduction reaction of Au ions. We strongly say that considering the surface modification of graphene as a catalyst, the development of functionalization for modifying the chemical, structural and electronic properties of graphene would find various applications in graphene-based biosensors.

3.2. Introduction

Graphene, atomically thin lattice of sp^2-hybridized carbon atoms in plane, has exceptional electronic, mechanical and thermal properties [1-3]. Modifying the basic electronic and chemical properties on the surface of graphene is critical for a variety of applications including electronic devices and biosensors[4-6]. The chemical functionalization (or 'dopping') of graphene is urgently important for enabling these applications and thus it has been explored for both covalent[7,8] and non-covalent[1,9,10] strategies (Table 3-1).

Covalent (Carrier Injection)		Non-covalent (Controlling the Fermi Level)	
Ad-atom doping	Functionalization	Gate dielectric	Physisorption
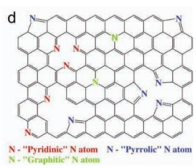	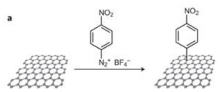	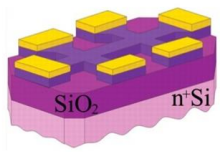	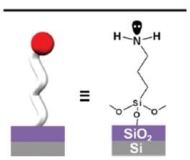
By changing carbon atom to other species such as boron or nitrogen	By breaking the sp2 bonding of graphene and make chemical bonding >Diazonium salts	Using a gate dielectric with changing a gate voltage	By chemical dopants on top or bottom of the graphene >SAM , HNO_3

Table 3-1. The graphene doping divided in covalent and non-covalent methods. [1,7-9]

First, covalent attachment of organic molecules onto the basal plane of graphene is intensively researched although it induces the decrease in its charge carrier mobility because not all applications need high charge carrier mobility[11]. Recently, the covalent bond between monolayer graphene and diazonium salts was influenced by underlying substrates due to different electron-hole charge fluctuation on each substrate[8]. Therefore, the functionalization of graphene is seriously affected by substrates.

The non-covalent interaction of a wide variety of molecules and materials with graphene has been studied extensively in the recent past[11]. These include organic molecules, inorganic materials, polymers, metal oxides and different types of nanoparticles[11,12]. In general, self-assembled monolayers (SAMs) have received considerable attention due to an ultrathin layer on oxide surface by self-assembly method[13], which related to the Fermi level of graphene easily tuned by attaching functional groups in SAMs[9]. For instance, SAMs with an amine ($-NH_2$) functional group have lone pair electrons and thus they exhibit electron-donation characteristics[9]. For this reason, graphene is n-type when graphene film is in contact with the NH_2-functional group in SAMs.

Thus, there should be possibility for the use of SAMs as a buffer layer to induce instantaneous doping of graphene and tune the density of electrons. Both functionalization of graphene with diazonium salts and SAMs can result in the opening of a bandgap[9,14,15] and tuning Fermi level[9,14] of graphene, which are desirable in the fabrication of electronic devices and bio applications (Figure 3-1).

Herein, we report the use of SAMs to control Fermi level of graphene for enhancing reactivity. Two types of SAMs with attaching functional groups ($-NH_2$, $-CH_3$) and bare SiO_2/Si substrate have an effect on the doping degree of graphene, which is related to Dirac voltage shift in transistor application. Also, the difference in reactivity on surface of graphene films by 4-Nitrobenzenediazonium (4-NBD) tetrafluoroborate was investigated by Raman spectroscopy which includes information of position, intensity and FWHM. Furthermore, the n-doped graphene as a catalyst shows that growth of gold particles is explained by the difference in reactivity compared to others due to electron-transfer.

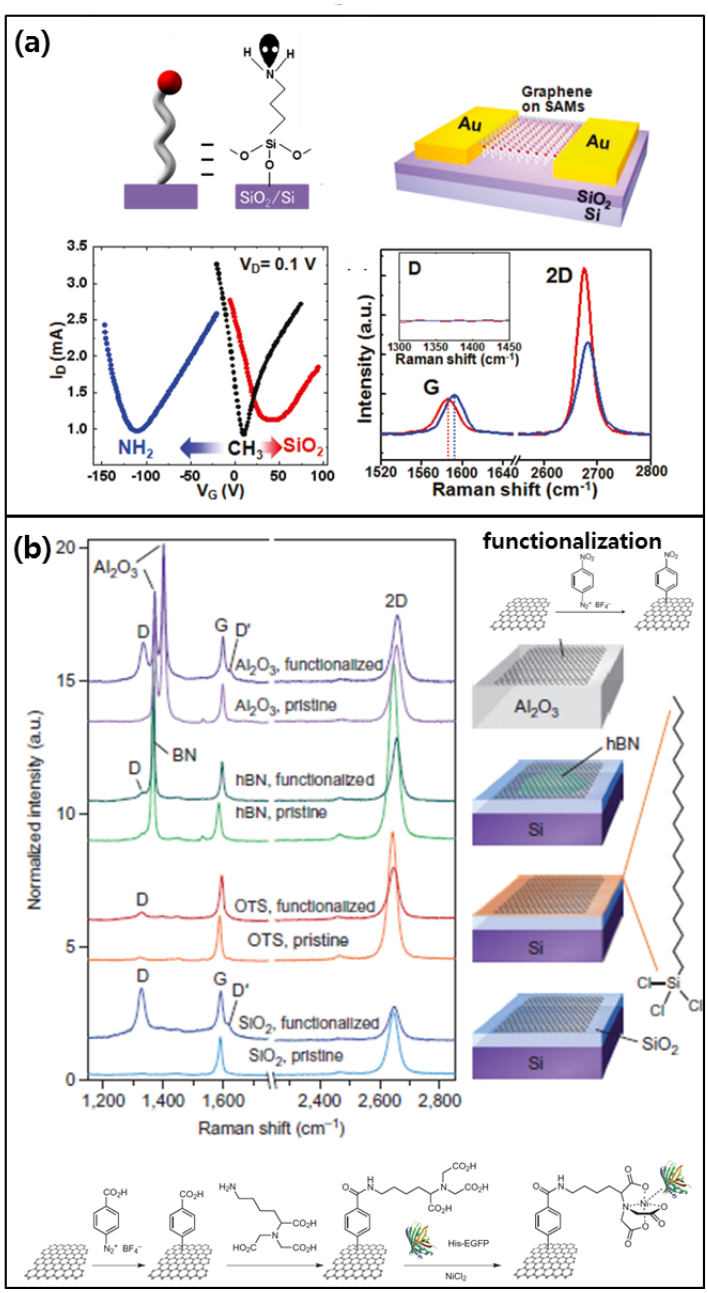

Figure 3-1. (a) Controlling Fermi level of graphene by APTES and analysis via field effect transistor and Raman spectroscopy. (b) The comparing reactivity on functionalization of graphene surface due to the properties of underlying substrates.

3.3. Experimental Section

Chemicals. Poly(methyl methacrylate) (PMMA), ammonium persulfate (APS), 3-aminopropyltrimethoxysilane (APTES, $-NH_2$ end group), Trichloro(octadecyl)silane (OTS, $-CH_3$ end group), 4-Nitrobenzenediazonium (4-NBD) tetrafluoroborate , sodium dodecyl sulfate (SDS) and Gold(III) chloride trihydrate from Sigma-Aldrich; acetone from Samchun Pure Chemicals; Deionized water from Purescience Ins.

CVD graphene growth and transfer. The graphene was synthesized on 23 um thick copper foil by Chemical Vapor Deposition (CVD) method, using a mixture of CH_4 (40 sccm) and H_2 (4 sccm) gases with vacuum pumping at 1000°C for 30 minutes. PMMA was spin-coated on one side of as-grown Cu foil, and the other side was removed by reactive ion etching (RIE). The Cu foil was etched with 80 mM of ammonium persulfate (APS) solution. After rinsing with distilled water, the graphene was transferred on target substrates then dried under 80°C. The samples were finally soaked in acetone to remove the PMMA layer.

Silanization and Device Fabrication. The NH_2-SAMs and CH_3-SAMs were constructed on SiO_2/Si (300nm) substrates by immersing 3-

aminopropyltrimethoxysilane (1:50) and Trichloro(octadecyl)silane (1:100) solution in toluene for 2 hours, respectively. After rinsed graphene/PMMA layers were trasnferred on two types of silanized substrates, PMMA was removed by acetone. For the fabrication of graphene field effect transistors, chromium (5nm) and gold (40 nm) electrodes were thermally deposited using pre-patterned masks which have same channel length (50 μm) and width (200 μm). Drain-source current (I_{ds}) was measured at constant drain-source voltage (V_{ds}) 10mV.

G Patterned SAMs by e-beam lithography. The SiO_2/Si substrate was patterned by using standard e-beam lithography. Resistor plays a role in blocking deposition of SAM s on the substrate. After the patterned substrate was silanized with APTES in distilled water solution, the resistor was removed in acetone[9].

Diazonium Functionalization of samples. Target samples with graphene were immersed in aqueous solutions of 10 mM 4-NBD tetrafluoroborate and 0.5 wt% sodium dodecyl sulfate (SDS) with mild stirring at 40 °C[8]. Most samples were reacted for 6 hours and patterned graphene was reacted for 30 minutes to compare I_D with I_G in Raman spectra. After several rinsing using distilled water, samples were blown dry with nitrogen.

Growth of Gold Particles on Substrates. Three kinds of substrates with graphene (-NH_2, -CH_3, SiO_2/Si) were soaked in 0.25 mM of $HAuCl_4 \cdot 3H_2O$ in 20 ml of distilled water at 30 °C for 3 hours. Then, they were rinsed several times in distilled water and blown with nitrogen gas.

Characterization. Raman spectra were obtained using a Raman spectroscopy (Renishaw 2000, excitation at 514.5 nm from an Ar ion laser). AFM was utilized to measure the hieght by a non-contact mode (Park System XE-100). Agilent 2602 was used for electrical measurement of field effect device in the ambient condition. SEM images were gained using SUPRA 55VP field-emission scanning electron microscopy (Carl Zeiss). Brightfiled and darkfield images were captured using optical microscopy (Nikon, Eclipse LV100ND). We captured dark field images under 400 ms of exposure time to compare in the same situation.

3.4. Results and Discussion

Electrochemical properties of graphene can be easily tuned by gases (water vapor, oxygen gas), chemicals or metals due to large exposed surface[2,10,16]. The types of doping are generally introduced in p-type and n-type, decided by withdrawing or donating electron groups[17]. After CVD graphene with PMMA support on copper foils was floated in ammonium persulphate solution, the graphene film was rinsed and transferred to SAMs-modified SiO_2/Si substrates constructed on SiO_2/Si (300nm) substrates by immersing 3-aminopropyltrimethoxysilane and Trichloro(octadecyl)silane solution, respectively (see detailed method in experiment section)[9].

Figure 3-2a shows a schematic illustration of molecular structures onto SiO_2 substrates, which relates doping types of graphene by the charge transfer process between different functional groups in SAMs and graphene[9]. APTES (NH_2-ending group) has negative charge whereas OTS (CH_3-ending group) has neutral charge compared to silicon oxide which has positive charge due to impurities[18].

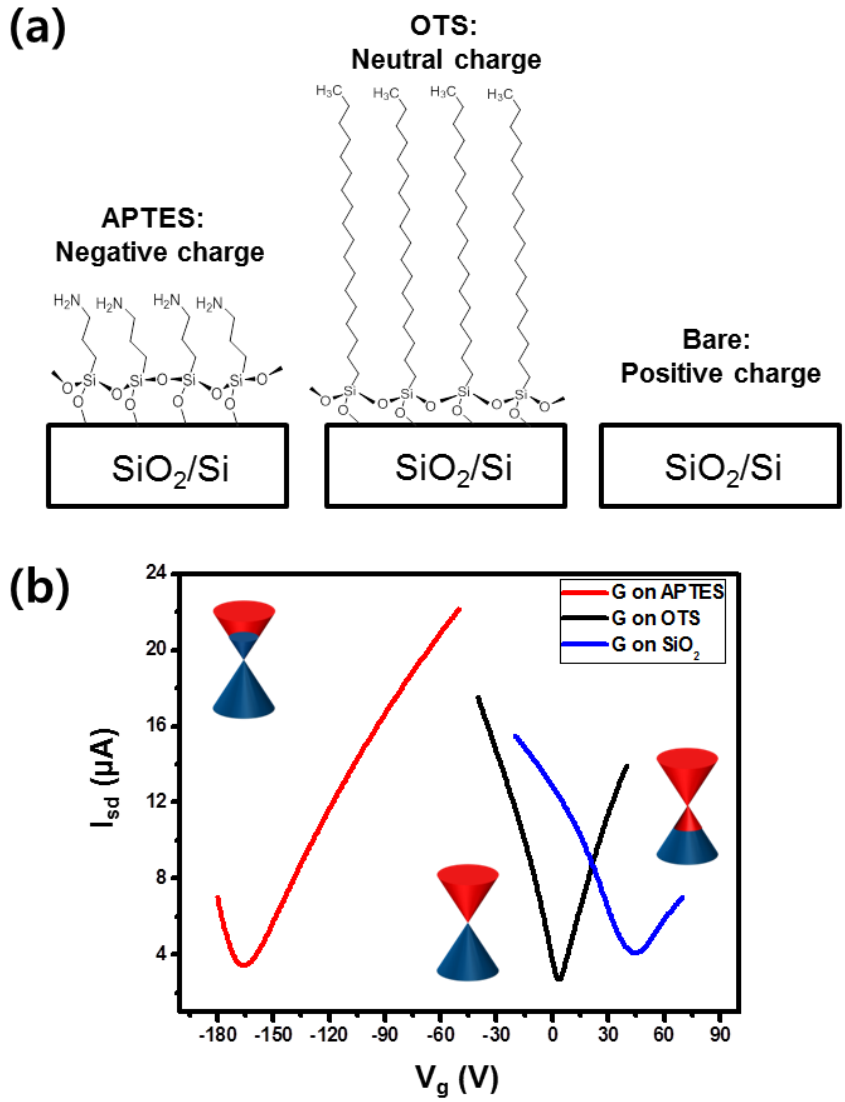

Figure 3-2. (a) Molecular structures of amine-functionalized SAMs and methyl-functionalized SAMs on SiO_2/Si substrates and bare SiO_2/Si substrate. (b) Current-voltage characteristics of the graphene FETs on different SAMs-modified substrates. V_g: gate voltage; I_{sd}: source-drain current.

The electrical properties of graphene films on modified-substrates can be measured via graphene field effect transistors (FETs) (Figure 3-2b). To examine the electrical performance of graphene films on different substrates, we fabricated graphene FETs with Au source/drain electrodes. The Dirac point, where electron and hole meet, is drastically changed according to the surface characteristics of the dielectric[9]. The Dirac point voltage is + 50 V at the surface of graphene on SiO_2, which is illustrated by p-doped graphene as previously discussed. Otherwise, the Dirac voltage is - 160 V for APTES, resulting from negative charge of NH_2-ending group in SAMs. For the CH_3-SAMs, the Dirac point shifts to a slightly positive value (+ 6 V) due to the effect of charge neutral. As these results, excess charge carriers induced by doping can be calculated by the equation[9,19].

$$n = \eta |V_n| \quad (1)$$

Where $\eta = 7.2 \times 10^{10}\ cm^{-2}\ V^{-1}$ and V_n is the Dirac point voltage. The excess charge carrier density of graphene on the NH_2-SAM/SiO_2, the CH_3-SAM/SiO_2 and bare SiO_2 are 1.15×10^{13} (electron), 4.32×10^{11} (hole) and 3.6×10^{12} (hole) cm^{-2}, respectively. These carrier concentrations are related to the Fermi energy level of the Dirac point by the equation[9,20].

$$E_f = \hbar v_F \sqrt{\pi n} \quad (2)$$

v_F = 1.1 × 10^6 ms^{-1} in the literature and n = charge carrier concentration[9,20]. The calculated the energy position of Dirac point is 0.43 eV for NH_2-SAM/SiO_2, 0.08eV for CH_3-SAM/SiO_2 and 0.24 eV for bare SiO_2. These values were fitted using correlation from the reference literature[21] shown in Figure 3-3.

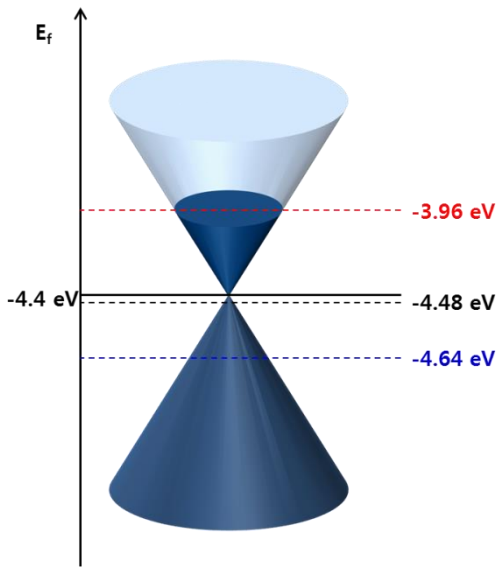

Figure 3-3. The illustration of calculated Fermi levels of each substrate by assuming -4.4 eV of standard graphene from the ref.20. Dashed lines indicate red: NH_2-SAM/SiO_2, black: CH_3-SAM/SiO_2, and blue: bare SiO_2.

To analyze the doping behavior of graphene on three types of substrates, we obtained representative Raman spectra[22,23] of the G and 2D bands from mapping data, as shown in Figure 3-4a. The G

and 2D bands are both strongly influenced by the carrier concentration and they have been extensively studied for doping characterization[25]. The width and position of the G band are changed according to doping. These changes are related to electron-phonon coupling and the Kohn anomaly[24]. The frequency of the G band reaches a minimum when the Fermi level is at the Dirac point[25]. The otherwise, G peak increases as the concentration of holes or electrons increases. Unfortunately, we could not explain well about 2D peak due to little change of 2D position (Figure 3-S1). In Figure 3-4a, n-doped graphene shows the blue shift of the G band and the decrease in 2D band intensity compared to others. These changes in peak position and intensity demonstrate that graphene are effectively doped by SAMs due to donating group[9]. As the results, we speculate that the strong n-doping effect by APTES has the most reactivity of chemical reaction due to abundant electron carriers.

Scatter plots of the Raman peak parameters are shown in Figure 3-4b-d. Data from literature reports of mechanically exfoliated monolayer graphene doped by electrostatic gating are included on these plots as comparisons[26,27]. Figure 3-4b shows the full-width at half-maximum (FWHM) of the G peak plotted against the position of the G peak. The black dashed line indicates that increasing n- or

p-doping leads to narrowing of the G peak and up-shift of the G peak position compared to references[22,23].

The integrated area intensity ratio $I_{2D/G}$ is plotted against G frequency in Figure 3-4c. It shows that the I_{2D}/I_G ratio decreases and position of G band increases corresponding to the increase of n- and p-doping because graphene on APTES is decreased by heavy doping effect compared to SiO_2. The G and 2D peak positions are plotted against each other with comparison data ref.41 to distinguish between n- and p-doping trends (Figure 3-4d). Graphene on OTS is on the p-doping branch but the bare graphene in our samples lies in the slightly p-doped region of this plot[27]. On the other hand, the scatters from graphene on APTES are on n-type branch[27].

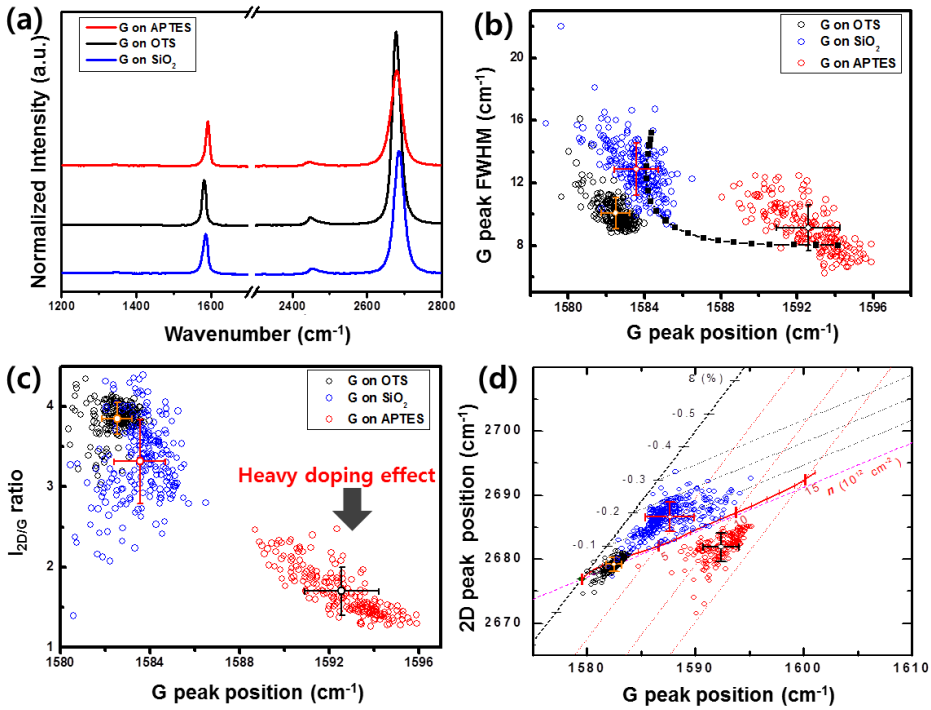

Figure 3-4. Spatial Raman maps were collected for graphene on each substrate for the 28 μm × 28 μm regions in different substrates with 125 points in each map. (a) Representative Raman spectra of monolayer graphene on different substrates (b) D peak full-width at half-maximum (FWHM) versus D peak position. (c) I_{2D}/I_G intensity ratio versus G peak position, with comparison data adapted from ref. 25 showing the doping trend. (d) 2D peak position versus G peak position distinguished literature[27]. Raman spectra were taken at 514 nm laser excitation wavelength.

Through electrical properties and the Raman graphs, we have confirmed that graphene on APTES is n-type[9]. As above results, we strongly believe that there is a large amount of electrons on n-doped graphene, which can act as an electron donor in chemical reactions. We expected that the reactivity was better when n-type graphene in oxidation-reduction reaction. To confirm our assumption about reactivity of graphene on different substrates, we tested diazonium functionalization (covalent bond) and gold particles (non-covalent bond) experiments. One was the covalent functionalization on patterned graphene, resulting in nitrobenzene groups being covalently attached to the n-type graphene[11]. The other was comparing the growth of gold particles on three types of substrates by electron-transfer effect.

Prior to the start, three types of graphene were compared by Raman maps. Figure 3-5a shows the representative Raman spectra of graphene on different substrates before and after 4-nitrovenzenediazonium (4-NBD) tetrafluoroborate functionalization [8]. As seen above, D peak of graphene on APTES was raised because of broken bonds from sp^2 to sp^3, which is key factor about the degree of reaction. In Figure 3-5b, the changes of I_D/I_G intensity ratio on different substrates were imaged. The rapid reaction at

graphene/APTES is inferred from these mapping images.

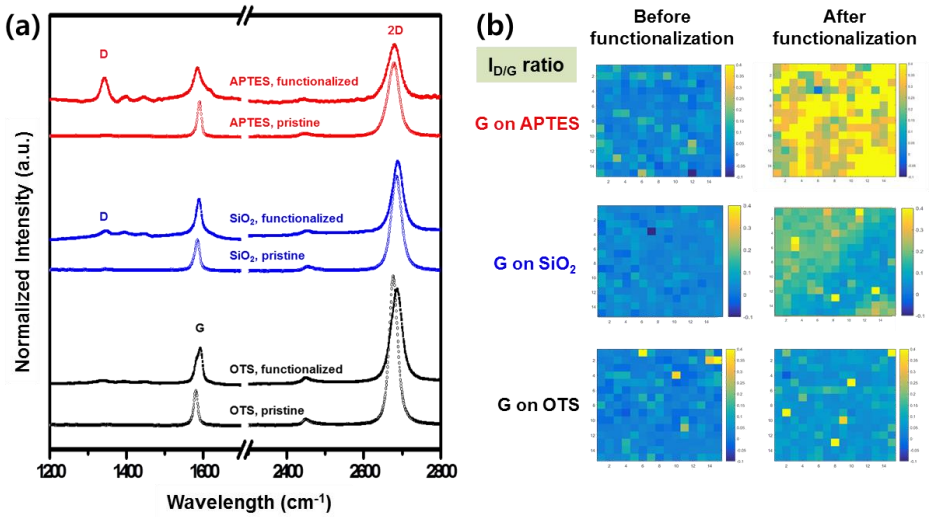

Figure 3-5. (a) Representative Raman spectra of CVD-grown graphene deposited on different substrates before and after diazonium functionalization, normalized to the G peak height. (b) Raman map of I_D/I_G intensity ratio according to different substrates before and after diazonium functionalization, respectively.

An exciting merit of doping using SAMs is its pattern ability[9]. To compare electrochemical reactivity on different electron density on graphene, we patterned alphabet G by e-beam lithography detailed in methods. SAMs can be patterned in a defined area by utilizing patterned e-beam resistor as blocking layer for SAMs

deposition[9]. Figure 3-S2 shows a schematic illustration of patterning process of graphene onto APTES on SiO_2/Si substrate. Graphene on NH_2-SAMs can be doped by the charge transfer process between functional group in SAMs due to lone pair electrons of amine groups, exhibiting electron donating characteristics[9]. For this reason, graphene is selectively n-doped on G pattern due to NH_2-functional groups in SAMs. Figure 3-6a,b show patterned substrate and graphene on NH_2-SAMs by optical image, respectively. Interestingly, intensity ratio of D and G (I_D/I_G) was dramatically changed because of the defect of graphene after covalent functionalization (Figure 3-6 c,d), indicating the difference in reactivity according to the property of a underlying substrate.

In addition, to obtain the reduction reactivity of gold ions on different substrates, we soaked the three graphene films into 0.25 mM of $HAuCl_4 \cdot 3H_2O$ in 20 ml of distilled water at 30 °C for 3 hours to grow gold nanoparticles (AuNPs) on graphene by electron-transfer. The optical and SEM images are shown in Figure 3-7a-i. As shown above, AuNPs are proportional to the amount of electron produced by the electrons on graphene. Therefore, the n-doped graphene with a large number of electrons is a critical factor for chemical reactions. It is explained by the Fermi level of graphene

which related to electron carriers as well as electron-hole charge fluctuation (puddling)[9]. We expect it to be used in applications such as biosensors or chemical sensors by surface enhance Raman spectroscopy, if the mechanism of metal growth is well revealed

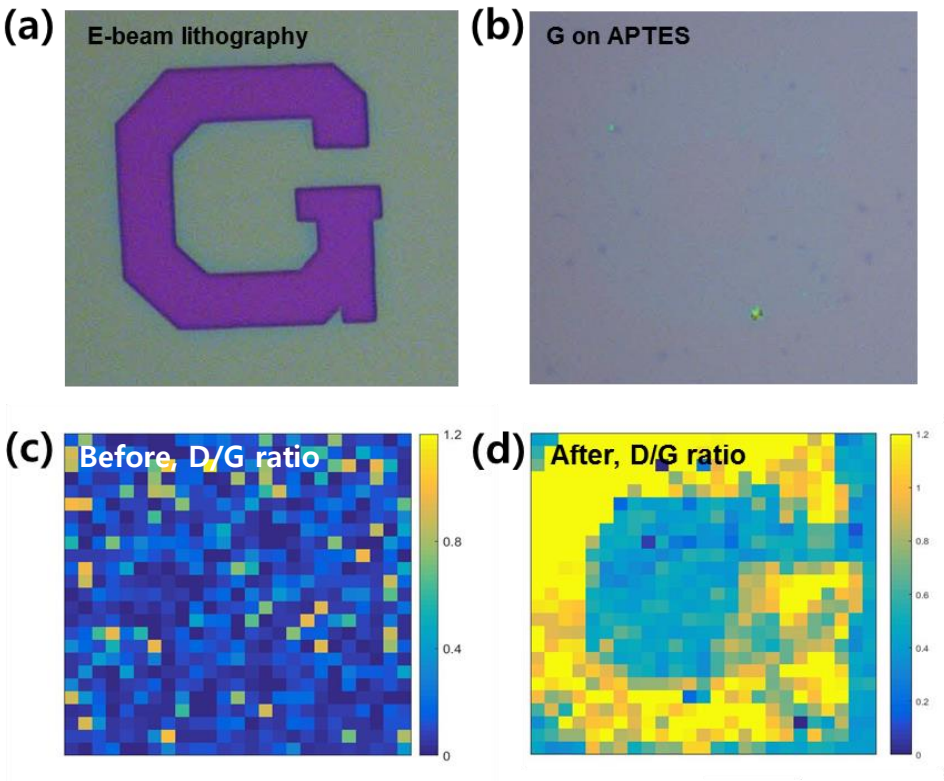

Figure 3-6. (a) Optical image of alphabet G patterned substrate by e-beam lithography. (b) Optical image of graphene on APTES patterned on SiO_2/Si substrate. (c) Raman map of I_D/I_G intensity ratio before functionalization (or after APTES pattern) (d) Raman map of I_D/I_G intensity ratio after covalently functionalization.

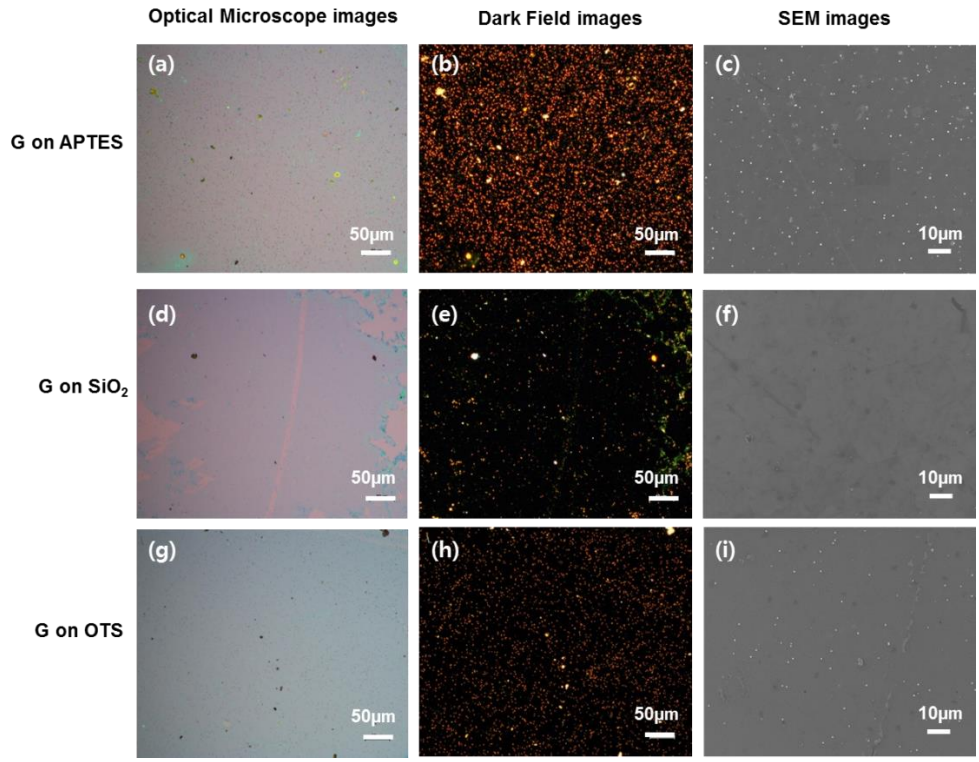

Figure 3-7. (a-c) Bright field, dark field and SEM images of numerous gold nanoparticles placed on graphene/APTES, respectively. (d-f) Bright field, dark field and SEM images of a few gold nanoparticles placed on graphene, respectively. (g-i) Bright field, dark field and SEM images of plenty of gold nanoparticles placed on graphene, respectively. Scale bars at the bottom right of each image.

3.5. Conclusion

In summary, the electron carriers of graphene depending on the functional ending groups in SAMs under graphene has been explored using FET and Raman spectroscopy. Graphene on NH_2-SAMs is more reactive towards covalent and non-covalent functionalization than graphene on CH_3-SAMs and bare SiO_2 due to donating group of NH_2. The reactivity is attributed to the amount of electrons on graphene surface. The difference in reactivity was shown by Raman maps before and after the reaction on patterned graphene/APTES substrate. Furthermore, a relative large of gold nanoparticles were synthesized on n-doped graphene than others. We expect that diazonium salts and gold ions are replaced with other attractive materials which can be used for potential for applications in sensors.

3.6. Supporting Information

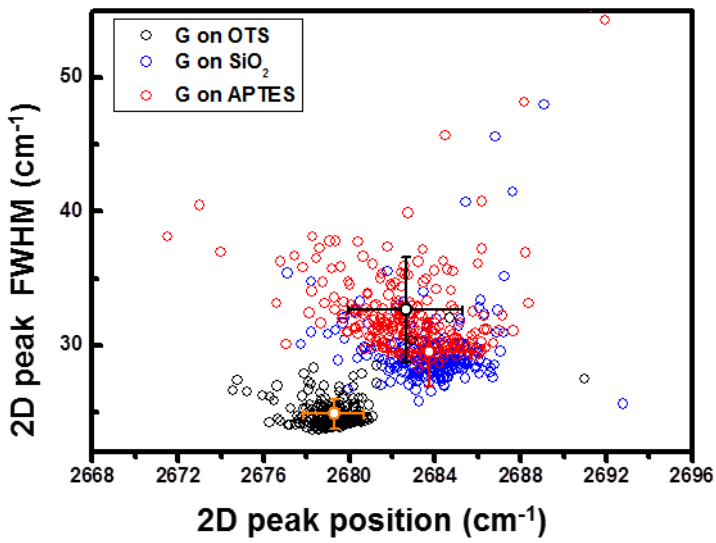

Figure 3-S1. 2D peak FWHM versus 2D peak position, showing different clusters depending on substrates.

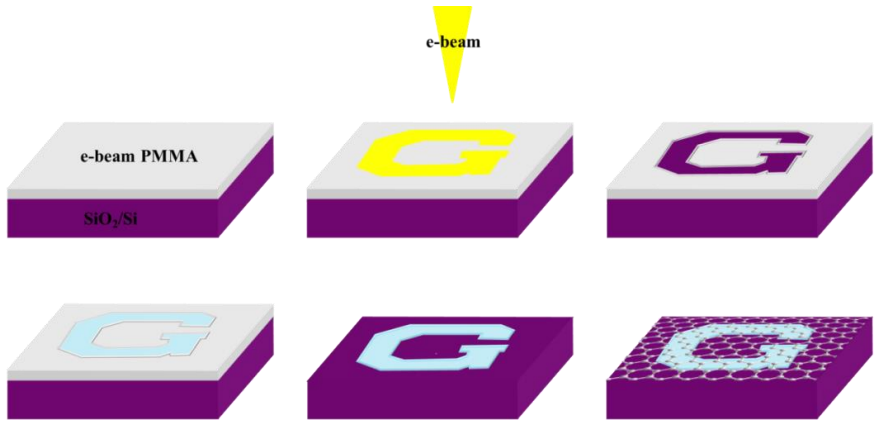

Figure 3-S2. The illustration of patterning process for alphabet G pattern using e-beam lithography. After patterned PMMA/SiO_2 immerged in APTES solution to block deposition of SAMs on the substrate, PMMA was removed in acetone. Then graphene was transferred onto SAMs-patterned substrate.

3.7. References

[1] S. Novoselov, A. K. Geim, S. V. Morozov, D. Jiang, Y. Zhang, S. V. Dubonos, I. V. Grigorieva and A. A. Firsov, *Science*, 2004, **306**, 666-669.

[2] A. K. Geim and K. S. Novoselov, *Nat. Mater.*, 2007, **6**, 183-191

[3] K. S. Novoselov, V. I. Falko, L. Colombo, P. R. Gellert, M. G. Schwab and K. Kim, *Nature*, 2012, **490**, 192-200

[4] Y. Shao, J. Wang, H. Wu, J. Liu, I. A. Aksay and Y. Lin, *Electroanalysis*, 2010, **22**, 1027-1036

[5] Q. He, S. Wu, Z. Yin and H. Zhang, *Chem. Sci.*, 2012, **3,** 1764-1772

[6] S. Pang, Y. Hernandez, X. Feng and K. Müllen, *Adv. Mater.,* 2011, **23**, 2779-2795

[7] S. Niyogi, E. Bekyarova, M. E. Itkis, H. Zhang, K. Shepperd, J. Hicks, M. Sprinkle, C. Berger, C. N. Lau, W. A. deHeer, E. H. Conrad and R. C. Haddon, *Nano Lett.*, 2010, **10**, 4061-4066

[8] Q. H. Wang, Z. Jin, K. K. Kim, A. J. Hilmer, G. L. C. Paulus, C.-J. Shih, M.-H. Ham, J. D. Sanchez-Yamagishi, K. Watanabe, T. Taniguchi, J. Kong, P. Jarillo-Herrero and M. S. Strano, *Nat. Chem.*, 2012, **4**, 724-732

[9] J. Park, W. H. Lee, S. Huh, S. H. Sim, S. B. Kim, K. Cho, B. H. Hong and K. S. Kim, *J. Phys. Chem. Lett.,* 2011, **2**, 841-845

[10] A. Krajewska, K. Oberda, J. Azpeitia, A. Gutierrez, I. Pasternak, M. F. Lopez, Z. Mierczyk, C. Munuera, W. Strupinski, *Carbon,* 2016, **100,** 625-631

[11] K. S. Mail; J. Greenwood; J. Adisoejoso; R. Phillipson; S. D. Feyter, *Nanoscale*, 2015, **7**, 1566

[12] V. Georgakilas, M. Otyepka, A. B. Bourlinos, V. Chandra, N. Kim, K. C. Kemp, P. Hobza, R. Zboril and K. S. Kim, *Chem. Rev.,* 2012, **112**, 6156-6214

[13] DiBenedetto, S. A.; Facchetti, A.; Ratner, M. A.; Marks, T. J. *Adv.Mater.* 2009, **21**, 1407-1433

[14] S. Niyogi, E. Bekyarova, M. E. Itkis, H. Zhan, K. Shepperd, J. Hicks, M. Sprinkle, C. Berger, C. N. Lau, W. A. deHeer, E. H. Conrad, and R. C. Haddon, *Nano Lett.*, 2010, **10**, 4061-4066.

[15] D. B. Farmer, R. Golizadeh-Mojarad, V. Perebeinos, Y. M. Lin, G. S. Tulevski, J. C. Tsang and P. Avouris. *Nano Lett.,* 2009, **9**, 388-392

[16] W. Chen, S. Chen, D. C. Qi, X. Y. Gao and A. T. S. Wee, *J. Am. Chem. Soc.*, 2007, **129**, 10418-10422

[17] F. M. Koehler, N. A. Luechinger, D. Ziegler, E. K. Athanassiou, R. N. Grass, A. Rossi, C. Hierold, A. Stemmer and W. J. Stark, *Angew. Chem.*, 2009, 48, 224-227

[18] Jang, Y.; Cho, J. H.; Kim, D. H.; Park, Y. D.; Hwang, M.; Cho, K. *Appl. Phys. Lett.* 2007, **90,** 132104

[19] Pisana, S.; Lazzeri, M.; Casiraghi, C.; Novoselov, K. S.;Geim, A. K.; Ferrari, A. C.; Mauri, F. *Nat. Mater.* 2007, **6**, 198–201.

[20] Zhang, Y. B.; Brar, V. W.; Wang, F.; Girit, C.; Yayon, Y.; Panlasigui, M.; Zettl, A.; Crommie, M. F. *Nat Phys.* 2008, **4**, 627–630.

[21] A. M. Zaniewski, C. J. Trimble, and R. J. Nemanich, *App. Phys. Lett.* 2015, **106**, 123104

[22] A. C. Ferrari, J. C. Meyer, V. Scardaci, C. Casiraghi, M. Lazzeri, F. Mauri, S. Piscanec, D. Jiang, K. S. Novoselov, S. Roth, and A. K. Geim. *Phys. Rev. Lett.* 2006, **97**, 187401

[23] Ferrari, A. C.. *Solid State Commun.* 2007, **143**, 47–57.

[24] Lazzeri, M. & Mauri, F. Nonadiabatic Kohn anomaly in a doped graphene monolayer. *Phys. Rev. Lett.* 2006, **97**, 266407

[25] R. Beams; L. G. Cancado; L. Novotny, J. Phys: Condens. Matter, 2015, **27**, 26

[26] Basko, D. M., Piscanec, S. & Ferrari, A. C,. *Phys. Rev. B,* 2009, **80**, 165413.

[27] A. Das1, S. Pisana, B. Chakraborty, S. Piscanec, S. K. Saha1, U. V. Waghmare, K. S. Novoselov, H. R. Krishnamurthy1, A. K. Geim, A. C. Ferrari and A. K. Sood. *Nature Nanotech.*, 2008, **3**, 210–215.

List of Publications

1. Sangmin Kang, Hae-Hyun Choi, Soo Bin Lee, Seong Chae Park, Jong Bo Park, Sangkyu Lee, Youngsoo Kim and Byunghee Hong, “Efficient Heat Generation in Large-Area Graphene Films by Electromagnetic Wave Absorption” *2D Mater.*, 2017, **4**, 025037

2. Sora Sin, Hae-Hyun Choi, Yung-Bin Kim, Byung Hee Hong, Joo-Young Lee, “Evaluation of Body Heating Protocols with Graphene Heated Clothing in a Cold” *International Journal of Clothing Science and Technology* [Accepted: 02-Jul-2017]

List of Presentations

1. Hae-Hyun Choi, and Byung Hee Hong, "Graphene Barrier Films by Dry Transfer Method for Blocking Degradation of Crystal Violet", *The 4th Korean Graphene and 2D Materials Symposium,* LOTTE Resort Buyeo, Korea (2017).

List of Patents

1. Sora Sin, Hae-Hyun Choi, Sangmin Kang, Joo-Young Lee, Byung Hee Hong, “Cold Protective Clothing Using Graphene Heater and Control Method Therof”, Registration number: 1016155910000 (2016.11.07)

2. Hae-Hyun Choi, Byung Hee Hong, Jong Hyun Park, “Photographs with Graphene Coating for Preventing Gases and Water”, (The procedure of application, 2017.06.28)

요약(국문 초록)

그래핀은 sp2 결합 된 탄소 원자의 두께의 층으로써 2004년 가임 등에 의해 실험적으로 설명되었다. 뛰어난 전기적, 화학적 및 기계적 특성으로 인해 스마트한 응용 분야에 대한 연구가 활발히 진행되어왔습니다. 여기서는 물리적 및 재료적 관점으로 화학기상증착법으로 성장한 그래핀 필름을 적용한 3가지 응용분야에 대해 논의합니다. 이 논문의 1 장, 2 장 그리고 3 장에 대한 간략한 개요가 아래에 나와 있습니다.

1 장에서는 그래핀 막을 이용하여 햇빛에 의한 유기 물질의 분해를 방지하여 색의 탈색을 막았습니다. 내구성을 확인하기 위해, 크리스탈 바이올렛 시료를 기판에 올리고 유브이 오존 환경에서 그래핀의 유무에 따라 크리스탈 바이올렛의 흡광도를 확인하였습니다. 여기서 그래핀이 없을 때 색소가 사라지는 결과를 얻을 수 있었습니다. 우리는 그래핀 벽이 염료의 산화를 막아 색상의 변화를 줄인다는 것을 발견하였습니다.

2 장에서는 우수한 열적 특성을 갖고 있는 그래핀을 이용하여 두 가지 그래핀 가열 메커니즘을 연구하고 실생활에 적용했습니다. 의복에 적용하는 연구에서는 효율적인 가열 프로토콜을 평가하고 신체부위에서 효과적인 열 전달 위치를 확인하기 위해 4층의 그래핀 히터를 제작하여 추운 환경에서 적용하였습니다. 다른 히터 메커니즘은 전자파의 흡수로 인해 그래핀 내에 전자의 움직임에 따라 온도가 올라가는 변화가 다르다는 것을 확인하였습니다. 이 독특한 메커니즘으로 서리를 없애는데 이용하기 위해 유리에 그래핀을 전사한 뒤 전자레인지에서 돌려 서리가 사라

지는 것을 확인하였습니다. 이러한 연구로부터 다양한 그래핀 응용이 학계 및 산업에서 많은 주목을 받길 바랍니다.

3 장에서는 전자의 이동 반응을 통해 자기 조립 단일층에 의한 그래핀의 페르미 레벨을 조절했습니다. 다른 말단 작용기를 가지고 있는 자기조립 단일층의 종류에 따라 그래핀의 전자 밀도에 영향을 치는 것을 통해 표면 작용화 반응과 금 나노 합성의 반응성의 차이를 확인 할 수 있었습니다. 흥미롭게도, N-도핑 된 그래핀은 다른 기판에 비해 그래핀 표면에서의 반응이 금 이온이 금 입자로 합성될 수 있도록 촉진해줍니다. 우리는 촉매로써의 그래핀이 금속 이온과 화학 반응에 전자를 제공하여 바이오 센서 등에 적용될 수 있음을 증명하였습니다.

주요어: 스마트 그래핀 응용, 화학기상증착, 자기조립막, 촉매, 막, 히터, 반응성

학번: 2015-20415